Jones matrix analysis for a polarization-sensitive optical coherence tomography system using fiber-optic components

B. Hyle Park, Mark C. Pierce, Barry Cense, and Johannes F. de Boer

Wellman Center for Photomedicine, Massachusetts General Hospital, Harvard Medical School, 50 Blossom Street, BAR 7, Boston, Massachusetts 02114

We present an analysis for polarization-sensitive optical coherence tomography that facilitates the unrestricted use of fiber and fiber-optic components throughout an interferometer and yields sample birefringence, diattenuation, and relative optic axis orientation. We use a novel Jones matrix approach that compares the polarization states of light reflected from the sample surface with those reflected from within a biological sample for pairs of depth scans. The incident polarization alternated between two states that are perpendicular in a Poincaré sphere representation to ensure proper detection of tissue birefringence regardless of optical fiber contributions. The method was validated by comparing the calculated diattenuation of a polarizing sheet, chicken tendon, and muscle with that obtained by independent measurement. The relative importance of diattenuation versus birefringence to angular displacement of Stokes vectors on a Poincaré sphere was quantified. © 2004 Optical Society of America

OCIS codes: 170.4500, 260.5430.

Optical coherence tomography is an interferometric technique capable of noninvasive imaging by measuring the intensity of light reflected from within tissue.[1] Polarization-sensitive optical coherence tomography (PS-OCT) provides additional contrast by observing changes in the polarization state of reflected light.[2–8] Simultaneous phase-resolved detection of interference fringes in two orthogonal polarization channels allows complete characterization of the reflected polarization state as Stokes vectors,[5] the evolution of which has been used to characterize birefringence and optic axis orientation in a variety of tissues.[9,10] Diattenuation can additionally be obtained through determination of the Jones and Mueller matrices from data acquired with bulk optic[6,11–13] and fiber-based[14] PS-OCT systems but with restrictions on the use of optical fiber components. In this Letter we present a Jones-matrix-based analysis capable of extracting birefringence, diattenuation, and relative optic axis orientation of a sample imaged with high-speed PS-OCT, with no restrictions on the use of optical fiber and nondiattenuating fiber-optic components. In addition, the use of optimal incident polarization states permits retrieval of birefringence under all circumstances. The method was validated with data from an IR polarizing sheet, chicken muscle, and tendon tissue.

The nondepolarizing polarization properties of an optical system can be completely described by its complex Jones matrix, $\mathbf{J}$, which transforms an incident polarization state, described by a complex electric field vector, $\mathbf{E} = [H \ V]^T$, to a transmitted state, $\mathbf{E}' = [H' \ V']^T$, and can be decomposed in the form $\mathbf{J} = \mathbf{J_R}\mathbf{J_P} = \mathbf{J_{P'}}\mathbf{J_{R'}}$, where $\mathbf{J_R}$ and $\mathbf{J_P}$ are the Jones matrices for a retarder and a polarizer, respectively.[15] Birefringence, described by $\mathbf{J_R}$, can be parameterized by three variables: a degree of phase retardation η about an axis defined by two angles, γ and δ. Diattenuation, described by $\mathbf{J_P}$, is defined as $d = (P_1{}^2 - P_2{}^2)/(P_1{}^2 + P_2{}^2)$ and can be parameterized by four variables, where P_1 and P_2 are the attenuation coefficients parallel and orthogonal, respectively, to an axis defined by angles Γ and Δ. These seven independent parameters, along with an overall common phase $\exp(i\psi)$, account for all four complex elements of a general Jones matrix $\mathbf{J}$. Assuming that birefringence and diattenuation in biological tissue share a common axis ($\delta = \Delta$ and $\gamma = \Gamma$),[13] the number of independent parameters is reduced by two. An incident and reflected polarization state yield three relations involving the two orthogonal amplitudes and the relative phase between them.[5] Therefore it is possible to use the six relationships defined by two unique pairs of incident and reflected states to exactly solve for the Jones matrix above.

A schematic of our fiber-based PS-OCT system is shown in Fig. 1. Assuming negligible diattenuation, the optical paths from the polarization modulator to the sample surface, described by $\mathbf{J}_{\mathrm{in}}$, and from the sample surface to the detectors, $\mathbf{J}_{\mathrm{out}}$, may be modeled as elliptical retarders. If the electric field after the polarization modulator is defined as $\mathbf{E}_{\mathrm{in}}$, then the electric field of detected light reflected from the surface of a sample is given by $\mathbf{E} = \exp(i\psi)\mathbf{J}_{\mathrm{out}}\mathbf{J}_{\mathrm{in}}\mathbf{E}_{\mathrm{in}}$. Defining the round-trip Jones matrix of the sample as $\mathbf{J}_S$, the detected light reflected from within the sample is given by $\mathbf{E} = \exp(i\psi')\mathbf{J}_{\mathrm{out}}\mathbf{J}_S\mathbf{J}_{\mathrm{in}}\mathbf{E}_{\mathrm{in}} = \exp(i\Delta\psi)\mathbf{J}_{\mathrm{out}}\mathbf{J}_S\mathbf{J}_{\mathrm{out}}{}^{-1}\mathbf{E}$, where $\Delta\psi = \psi' - \psi$. Since the Jones matrices for elliptical retarders are unitary and thus form a closed group, we can rewrite the combined Jones matrix $\mathbf{J}_T \equiv \mathbf{J}_{\mathrm{out}}\mathbf{J}_S\mathbf{J}_{\mathrm{out}}{}^{-1} = \mathbf{J}_U[P_1 \exp(i\eta/2), 0; 0, P_2 \exp(-i\eta/2)]\mathbf{J}_U{}^{-1}$, using $\mathbf{J}_U = \exp(i\beta) \times \{C_\theta \exp[i(\phi - \varphi)], -S_\theta \exp[i(\phi + \varphi)]; S_\theta \exp[-i(\phi + \varphi)], C_\theta \exp[-i(\phi - \varphi)]\}$ (Ref. 16) to describe a general unitary transformation, where $C_\theta = \cos\theta$ and $S_\theta = \sin\theta$.

A recently described method for obtaining the full polarization parameters of a sample with fiber-based PS-OCT imposed the condition that the round-trip
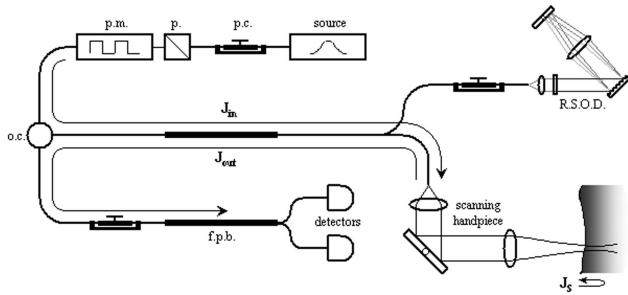
Fig. 1. Schematic of the fiber-based PS-OCT system: p.c., polarization controller; p., polarizer; p.m., polarization modulator; o.c., optical circulator; R.S.O.D., rapid-scanning optical delay; f.p.b., fiber polarizing beam splitter. $\mathbf{J}_{in}$, $\mathbf{J}_{out}$, and $\mathbf{J}_S$ are the Jones matrix representations for the one-way optical path from the polarization modulator to the scanning handpiece, the one-way optical path back from the scanning handpiece to the detectors, and the round-trip path through some depth in the sample, respectively.

Jones matrix for light returning from the sample surface must be transpose symmetric.[14] The algorithm required that any fiber-optic components be traversed in a round-trip manner to cancel any inherent circular birefringence, to ensure $\delta = \Delta = 0$ and achieve transpose symmetry. This restricts the placement of optical fiber and requires a bulk beam splitter in the interferometer instead of a fiber-optic splitter. In the formulation proposed here, transpose symmetry of the overall Jones matrix is not required, permitting the use of nondiattenuating fiber-optic components, such as splitters and circulators, as well as removing any restrictions on the use of fiber throughout the system.

We can obtain an alternative formulation for $\mathbf{J}_T$ by combining information from two unique incident states, $[H_1' \quad H_2'; V_1' \quad V_2'] = \exp(i\Delta\psi_1) \times \mathbf{J}_T[H_1 \quad \exp(i\alpha)H_2; V_1 \quad \exp(i\alpha)V_2]$, where $\alpha = \Delta\psi_2 - \Delta\psi_1$.[12] The polarization parameters of interest can be obtained by equating the two expressions for $\mathbf{J}_T$ to yield

$$\exp(i\Delta\psi_1)\begin{bmatrix} P_1\exp(i\eta/2) & 0 \\ 0 & P_2\exp(-i\eta/2) \end{bmatrix}$$

$$= \begin{bmatrix} C_\theta & S_\theta \\ -S_\theta & C_\theta \end{bmatrix}\begin{bmatrix} \exp(-i\phi) & 0 \\ 0 & \exp(i\phi) \end{bmatrix}\begin{bmatrix} H_1' & H_2' \\ V_1' & V_2' \end{bmatrix}$$

$$\times \begin{bmatrix} H_1 & \exp(i\alpha)H_2 \\ V_1 & \exp(i\alpha)V_2 \end{bmatrix}^{-1}\begin{bmatrix} \exp(i\phi) & 0 \\ 0 & \exp(-i\phi) \end{bmatrix}$$

$$\times \begin{bmatrix} C_\theta & -S_\theta \\ S_\theta & C_\theta \end{bmatrix}. \tag{1}$$

In principle, parameters θ, ϕ, and α can be solved for with the condition that the off-diagonal elements of the matrix product on the right-hand side of Eq. (1) are equal to zero. In practice, real solutions cannot always be found, as measurement noise can induce nonphysical transformations between incident and transmitted polarization states. To account for this we optimize parameters α, ϕ, and θ to minimize the sum of the magnitudes of the off-diagonal elements. A relative optic axis can be derived from ϕ and θ, given in Stokes parameter form by $\mathbf{A} = [1 \quad C_{2\phi}S_{2\theta} \quad C_{2\phi}S_{2\theta} \quad S_{2\phi}]^T$.[14,17] The degree of phase retardation can easily be extracted through the phase difference of the resulting diagonal elements, and the diattenuation by their magnitudes. The error on the calculation can be estimated by taking the ratio of the sum of the magnitudes of these off-diagonal elements to the sum of the magnitudes of the diagonal elements.

As mentioned above, $\mathbf{J}_T$ can be determined experimentally by using two unique incident polarization states to probe the same volume of a sample. However, when two orthogonal incident polarization states are used,[14] birefringence cannot be retrieved under all circumstances.[18] A better choice is to use two incident polarization states perpendicular in a Poincaré sphere representation[9,10,17,19,20] to guarantee that polarization information can always be extracted.

Details of the all-fiber-based PS-OCT system, capable of imaging 2048 depth scans per second, used to verify this analysis were presented by Pierce et al.[19] PS-OCT images were taken of an IR polarizing sheet, orthogonal to the axis of the incident beam, and rotated in 10° increments about this axis, spanning a full 360°. An average single-pass diattenuation value derived from the scans of 0.992 ± 0.002 is in reasonable agreement with an independent measurement of 0.996 ± 0.001, determined by transmission of linearly polarized light, parallel and orthogonal to the optic axis of the sheet. The optic axis determination is shown in Fig. 2, in which the optic axis orientation is plotted with respect to the set orientation of the polarizing sheet. The inset illustrates that the optic axes are nearly coplanar and span two full circles on the Poincaré sphere, in agreement with the imaging geometry.

As a control measurement, a series of OCT intensity images with varying single linear incident polarization states were acquired from chicken tendon and muscle tissue. The orientations for which the reflected polarization state from within the tissue
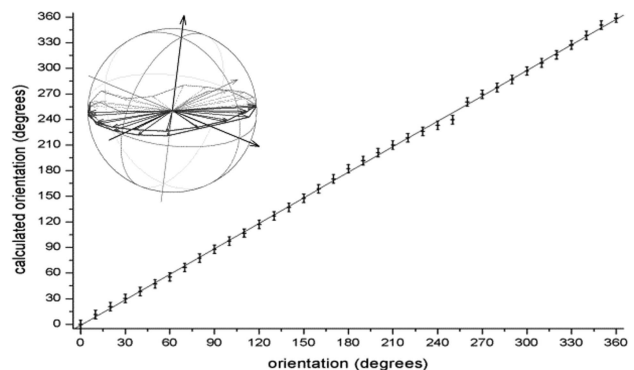

Fig. 2. Plot of the PS-OCT-derived relative optic axis orientation of a polarizing sheet as a function of its set orientation. Inset, the same optic axes plotted on a Poincaré sphere.
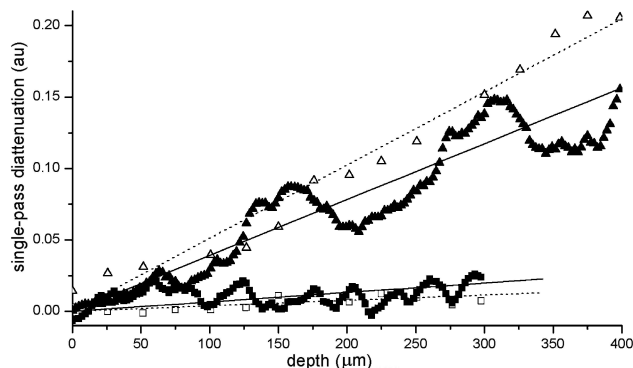
Fig. 3. Single-pass diattenuation as a function of depth. The open triangles and squares represent control diattenuation values of chicken tendon and muscle, respectively, calculated from comparison of the reflectivity profiles for linear incident polarization states along and orthogonal to the fiber direction. The solid triangles and squares are diattenuation values derived from PS-OCT images acquired from the same tissues. Linear least-squares fits are shown for all plots.

varied minimally as a function of depth were chosen as those where the incident state was aligned parallel or orthogonal to the sample optic axis. The corresponding intensity profiles described attenuation parameters P_1 and P_2, from which depth-resolved control diattenuation plots were derived. PS-OCT scans were then acquired of the same tissue regions. After correcting for slight imbalances between the gains of the two orthogonal detectors, depth-resolved plots of both diattenuation and phase retardation were calculated. The resulting single-pass diattenuation plots are displayed in Fig. 3. Numerical simulation revealed that the average angular displacement of a state on the Poincaré sphere for a small diattenuation, d, is approximately $(40d)°$. Given that a standard deviation of the order of $5°$ for individual polarization states reflected from the surface was found, the control and PS-OCT-derived diattenuation per unit depth of chicken muscle, 0.0380 ± 0.0036/mm versus 0.0662 ± 0.0533/mm, and tendon, 0.5027 ± 0.0353/mm versus 0.3915 ± 0.0365/mm, were within reasonable agreement. These diattenuation values correspond to angular displacements of the order of $1.5-2.5°$/mm and $15-20°$/mm for muscle and tendon, respectively. The slopes of the phase retardation plots, $179.7°$/mm for muscle and $1184.4°$/mm for tendon, are well within expected parameters. The angular displacements of the Stokes vectors as a result of diattenuation are negligible compared with those of birefringence in both cases, implying that for these samples birefringence can be determined with accuracy, even ignoring diattenuation. This was confirmed by applying a previously described method,[9] that yielded similar slopes of $211.9°$/mm and $1212.5°$/mm for muscle and tendon, respectively.

In conclusion, we have developed a new polarization analysis capable of extracting birefringence, diattenuation, and common relative optic axis orientation for a PS-OCT system with the unrestricted use of nondiattenuating fiber-optic components. This information was extracted by probing samples with incident polarizations that alternated between states that were perpendicular in a Poincaré sphere representation to ensure proper detection of birefringence. The method was verified experimentally, and demonstrated that, in chicken tendon and muscle, the angular deviations of Stokes parameters on a Poincaré sphere that are due to diattenuation are negligible compared with those that are due to birefringence.

References

1. D. Huang, E. A. Swanson, C. P. Lin, J. S. Schuman, W. G. Stinson, W. Chang, M. R. Hee, T. Flotte, K. Gregory, C. A. Puliafito, and J. G. Fujimoto, Science **254,** 1178 (1991).
2. J. F. de Boer, T. E. Milner, M. J. C. van Gemert, and J. S. Nelson, Opt. Lett. **22,** 934 (1997).
3. J. F. de Boer, S. M. Srinivas, A. Malekafzali, Z. Chen, and J. S. Nelson, Opt. Express **3,** 212 (1998), http://www.opticsexpress.org.
4. M. J. Everett, K. Schoenenberger, B. W. Colston, and L. B. Da Silva, Opt. Lett. **23,** 228 (1998).
5. J. F. de Boer, T. E. Milner, and J. S. Nelson, Opt. Lett. **24,** 300 (1999).
6. G. Yao and L. V. Wang, Opt. Lett. **24,** 537 (1999).
7. C. K. Hitzenberger, E. Gotzinger, M. Sticker, M. Pircher, and A. F. Fercher, Opt. Express **9,** 780 (2001), http://www.opticsexpress.org.
8. J. F. de Boer and T. E. Milner, J. Biomed. Opt. **7,** 359 (2002).
9. C. E. Saxer, J. F. de Boer, B. H. Park, Y. H. Zhao, Z. P. Chen, and J. S. Nelson, Opt. Lett. **25,** 1355 (2000).
10. B. Cense, T. C. Chen, B. H. Park, M. C. Pierce, and J. F. de Boer, Opt. Lett. **27,** 1610 (2002).
11. S. L. Jiao, G. Yao, and L. H. V. Wang, Appl. Opt. **39,** 6318 (2000).
12. S. L. Jiao and L. V. Wang, J. Biomed. Opt. **7,** 350 (2002).
13. S. L. Jiao and L. H. V. Wang, Opt. Lett. **27,** 101 (2002).
14. S. Jiao, W. Yu, G. Stoica, and L. V. Wang, Opt. Lett. **28,** 1206 (2003).
15. J. J. Gil and E. Bernabeu, Optik **76,** 67 (1987).
16. G. Arfken, *Mathematical Methods for Physicists* (Academic, San Diego, Calif., 1985).
17. B. H. Park, C. Saxer, S. M. Srinivas, J. S. Nelson, and J. F. de Boer, J. Biomed. Opt. **6,** 474 (2001).
18. B. H. Park, M. C. Pierce, and J. F. de Boer, "Comment on 'Optical-fiber-based Mueller optical coherence tomography,'" Opt. Lett. (to be published).
19. M. C. Pierce, B. H. Park, B. Cense, and J. F. de Boer, Opt. Lett. **27,** 1534 (2002).
20. B. H. Park, M. C. Pierce, B. Cense, and J. F. de Boer, Opt. Express **11,** 782 (2003), http://www.opticsexpress.org.